PROCEEDINGS OF SPIE

SPIEDigitalLibrary.org/conference-proceedings-of-spie

An integrated 1-5 micron test bench for the characterization of cryogenic optical elements

Udo J. Wehmeier, Jarron Leisenring, Olivier Durney, Elliott Solheid, Gerard A. Luppino, et al.

Udo J. Wehmeier, Jarron Leisenring, Olivier Durney, Elliott Solheid, Gerard A. Luppino, Michael R. Meyer, "An integrated 1-5 micron test bench for the characterization of cryogenic optical elements," Proc. SPIE 8446, Ground-based and Airborne Instrumentation for Astronomy IV, 84463G (24 September 2012); doi: 10.1117/12.927066

SPIE.

Event: SPIE Astronomical Telescopes + Instrumentation, 2012, Amsterdam, Netherlands

An Integrated 1-5 Micron Test bench for the Characterization of Cryogenic Optical Elements.

Udo J. Wehmeier[a], Jarron Leisenring[a], Olivier Durney[b], Elliott Solheid[b],
Gerard A. Luppino[c], Michael R. Meyer[a]
[a]Institute for Astronomy, ETH Zürich, 8093 Zürich, Switzerland
[b]Orion Labs, LLC, Tucson, AZ, USA
[c]GL Scientific, Inc., Honolulu, HI, USA

ABSTRACT

We report on the final design and current status of a 1-5 micron infrared test bench at the ETH Zurich Institute for Astronomy. This facility will enable us to characterize infrared optics, both reflective and transmissive, at cryogenic operating temperatures for both ground- and space-based applications. A focus of our lab is to facilitate the detection and characterization of extra-solar planets. The test bench is designed to characterize a range of spectrally dispersive and diffraction suppression optics such as filters, grisms, gratings, as well as both focal and pupil plane coronagraphs. The test bench is built around a 2048x2048 HAWAII-2RG detector from Teledyne Imaging Systems. The optical bench is envisioned to operate down to 30 K. "First light" is expected in the second half of 2012. We outline the status of the project, and describe the capabilities of the test bench in detail in order to alert potential collaborators to this new capability.

Keywords: optics, performance testing, infrared detectors, exoplanet detection, coronagraphs

1. INTRODUCTION

For over twenty years, rapid advances in infrared array detectors have fueled innovation in infrared instrumentation for both ground- and space-based applications. The maturation of adaptive optics and continued investment in space-based platforms such as the James Webb Space Telescope has also played a strong role. This extraordinary pace of innovation has also led to the development of novel optics, such as systems for spectral dispersion and diffraction suppression, in the 1-5 micron regime. Conceiving of, designing, and bread-boarding a novel optical system is just the first step towards demonstrating the achievement of performance goals. Laboratory testing of new IR optics can be a crucial part of the development program before final "on-sky" validation. In addition to providing efficient exploration of a concept under study such laboratory testing can save valuable engineering time at the world's most powerful (and expensive) telescopes. Such laboratory testing of optical components is also best done under conditions that reflect as accurately as possible the conditions of use. Here we describe our efforts to create a cryogenic test bench that can be used to explore the quality of infrared optics from 1-5 microns. Focus on this wavelength range, as well as spectrally dispersive and diffraction suppression optics, was driven by the scientific interests of the Star and Planet Formation Research Group at the Institute for Astronomy, ETH Zurich. It is our hope that such a capability will be useful to a broad segment of the community invoved in the design and development of infrared instrument for both ground- and space-based applications.

2. TEST BENCH OVERVIEW

In this section we give a general overview of the system and describe the functional requirements we articulated that drove our design choices. The goal was to design a cryogenic optical test bench (CTB) to operate from 1-5 microns. We want to be able to test diffraction suppression optics, such as apodizing phase plates[1], as well as reflection gratings, a range of wide, intermediate, and narrow-band filters, transmission grisms, as well as other optical components. The test bench consists of three main components: a large cryostat for the optical test optics designated as the optical test bench (OTB); a modular 1-5 micron (hereafter NIR) camera designed by GLS; and a modular NIR light source (LS). Together

Ground-based and Airborne Instrumentation for Astronomy IV, edited by Ian S. McLean, Suzanne K. Ramsay,
Hideki Takami, Proc. of SPIE Vol. 8446, 84463G · © 2012 SPIE · CCC code: 0277-786X/12/$18 · doi: 10.1117/12.927066

these three components constitute an end-to-end system that is capable of testing a variety of optical components and subsystems at cryogenic temperatures.

We wanted to accommodate pupil plane optics up to 2 inch outer diameter, and cryogenic filters of 1 or 2 inch outer diameter. The test bench can accommodate coronographs in either a pupil or focal plane configurations, with appropriate field stops and Lyot stops including two collimated optical beams. We also foresee other uses of the test setup, such as detector characterization for any HAWAII-2RG (H2RG) format focal plane array (FPA). Outfitted with the latest incarnation of Teledyne's SIDECAR ASIC readout electronics, this setup has the further capability to take full advantage of the multiple modes and readout schemes built into the H2RG readout circuitry.

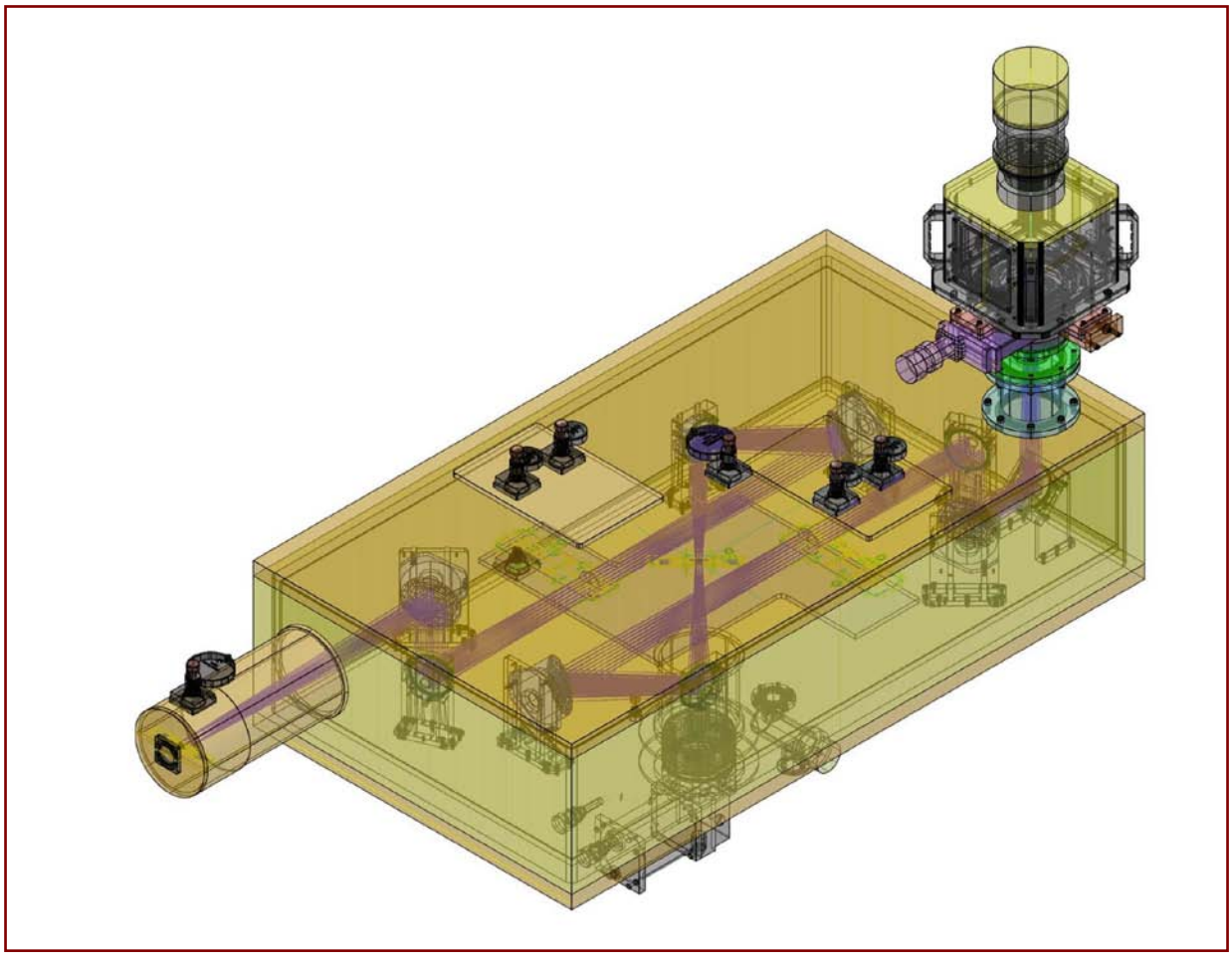

Figure 1. CAD model of the CTB showing the main OTB cryostat, top-mounting camera and input port (left). Measurements are approximately 1.6x0.8x1.5m (LxWxH).

2.1 Functional requirements for OTB

The initial requirements for the OTB are given by the criteria discussed above. They are selected for maximum flexibility within our lab budget and to accommodate as many possible optics as we could anticipate.

1. Wavelengths of operation for test set-up are 1-5 microns.
2. Ability to test transmissive and reflective optical elements
3. Ability to test up to 2-inch elements at two (2) independent pupil planes.

4. Ability to reimage the object plane with a ratio of approximately 1:1.
5. Include an intermediate focal plane in between the pupil planes.
6. Optical quality will be characterized as surface figure, with a goal of 15nm RMS for any fold mirror and 63nm RMS for the powered optics. (measured at 632.8nm)
7. The PSF should be oversampled by at least 2, but not greater than 10. A goal of 3-4 pixels for the diffraction limited FWHM at 3 microns is requested.
8. A pupil-reimaging lens will be designed for input pupil inspection.
9. Optimize for the following options in terms of cost, performance, complexity and risk.
    a. Off-axis paraboloids versus bi-conic optical design
    b. Folded versus unfolded design with regards to minimum achievable temperatures.
    c. Assessment of operational complexity including core competencies required for efficient operation.
    d. Assessment of running costs per annum (expendables and anticipated replacements).
10. Integrated NIR light source or external monochromator input user selectable
11. Goal of having NIR camera detach for use with other projects or telescopes.

The initial design of the OTB concept involved two design studies which attempted to satisfy these functional requirements within the allotted budget. There were several iterations of the optical concept as well as the camera design and hardware infrastructure. In the following sections we will present the design philosophy and the choices made to arrive at our final design.

3. SELECTION OF CAMERA

3.1 Requirements for the NIR camera

As the goal of the OTB is to test high precision optics at the limit of current technology for ground and space instrumentation, the NIR camera was specified to be of the highest sensitivity and stability our budget would allow. Other considerations, such as the required operating temperature of the FPA and the selection of front end and support equipment were factored into this decision. We sought a high performance 1-5 micron detector in terms of maximum sensitivity, low dark current, modest read noise, and stability over time. We also consider modularity of the camera cryostat an advantage, as well as a high level of integration and product maturity on the front-end electronics. The desired assembly must demonstrate high reliability and reduced level of technical support for routine operation.

3.2 1-5 micron detector selection

Our search for a suitable FPA to cover the 1-5 micron band was extensive and covered a number of detectors, some with high dark currents and affordable cost, as well as more costly solutions which have extremely good sensitivity and dark current behavior. An strong consideration was operating temperature of the detector and implications for complexity, cost and risk. In view of this goal, InSb FPAs were considered, but were not preferred as a result of their more significant cooling needs, as well as the low level of integration of the front ends available. Ultimately, it was determined that selecting a modern HgCdTe detector was the best possible choice. We were happy to accept delivery of a 5.3-micron cutoff H2RG detector from Teledyne Scientific Instruments in Camarillo, CA. This FPA was selected in tandem with the cryogenic SIDECAR front end (FE) to control the detector.

The selection of the SIDECAR front end ASIC will allow us the option to run the H2RG, which is a 2048x2048 pixel device, up to 38Hz frame rate. This cryogenic ASIC is available in a configuration to run inside the camera cryostat which results in an extremely compact and reliable packaging option. In addition, Teledyne offered a new interface electronics module, the SAM (SIDECAR Acquisition Module), which replaces the JADE2 interface (originally developed for the JWST program). The new SAM interface will allow the SIDECAR ASIC a variety of options to communicate with the host computer via USB, as well as CamLink and GigE protocols.

3.3 Selection of camera cryostat package

The modularity of the NIR camera is important, given the level of investment in the hardware and the desire to use this camera in other configurations. We selected an integrated camera cryostat developed by GL Scientific (GLS) in Honolulu, HI to house our H2RG detector and SIDECAR electronics. This compact camera will maintain constant temperatures from less than 70K to 150K at the FPA using the integrated Stirling cryocooler. As a result, this camera meets our requirements as described in the above section very well. The GLS camera model SCC-g2 is designed to house the 5.3 micron cutoff H2RG FPA, cryogenic SIDECAR ASIC, and vacuum feedthroughs to the SAM electronics. The size of the compact cryostat is approximately 275mm by 275mm by 425mm and weighs less than 30kg.

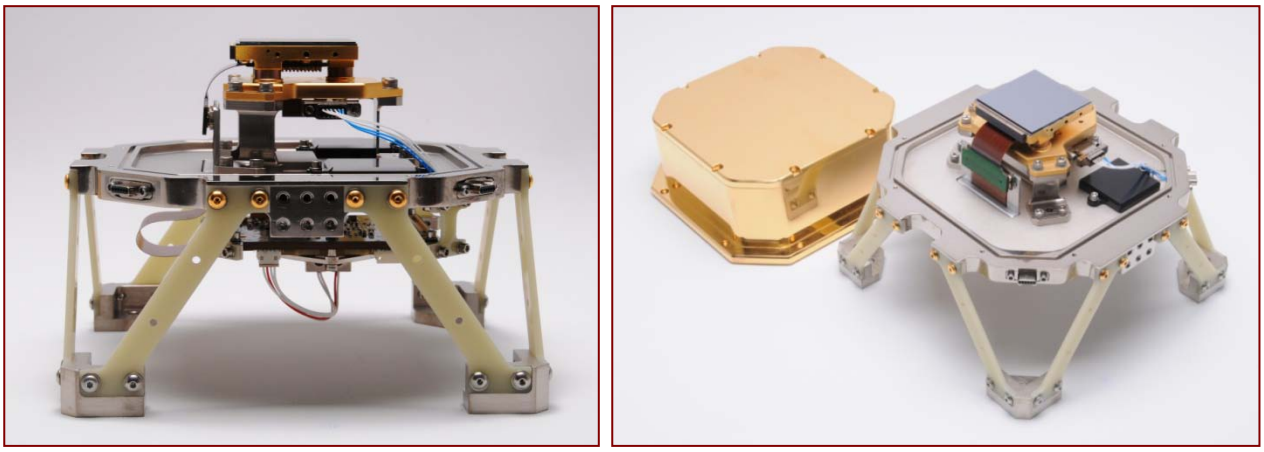

Figure 2. Photos of the H2RG on its molybdenum mounting plate attached to the inner sanctum baseplate. The SIDECAR ASIC PCB is visible at the left and the gold-plated cover and blank-off lid on the right. Outer dimensions are approximately 275x275x425mm.

3.4 Camera Cryocooler and Internals

The GLS SCC-g2 is designed around a CryoTel GT free-piston Stirling cryocooler manufactured by Sunpower, Inc., Athens OH. The CryoTel GT has a rated heat lift of 15W at 77K temperature with a low-end temperature limit of approximately 45K. With this cryocooler, the cryostat can maintain the H2RG SCA temperature below 70K and the SIDECAR ASIC temperature at 150K under normal operating conditions. Higher operating temperatures are possible by adjusting the cryocooler temperature setpoint and employing heaters at various locations in the temperature chain.

The H2RG detector is mounted to a molybdenum plate attached by flexure standoffs to an aluminum "inner sanctum" (IS) baseplate (see Figure **2**). The inner sanctum has a light-tight cover with interchangeable lids (blank for detector-limited dark frames, or perforated for attaching in a light-tight fashion to upstream optics). A light-tight flexcircuit feedthrough pierces the IS baseplate and connects the detector to the SIDECAR ASIC PCB suspended under (and thermally isolated from) the IS baseplate. Another flexcircuit mates to the output side of the SIDECAR ASIC PCB and passes through the radiation shield and vacuum bulkhead to the externally-mounted Teledyne interface electronics (SAM). The IS baseplate is thermally connected to the cryocooler head via two sets of thermal straps. The straps are made of a stack of thin copper foils and are arranged so they minimize any vibrational coupling from the cryocooler head to the detector. Separate, smaller thermal straps are connected to the SIDECAR ASIC. These smaller straps are sized so the SIDECAR ASIC will equilibrate near the desired operating temperature of 150K, thus minimizing the amount of power needed for the ASIC heater.

Temperature sensors and heaters are located at the SCA mounting plate, the inner sanctum baseplate, and the SIDECAR ASIC. A Lakeshore Cryotronics Model 336 4-channel temperature controller is used to set and regulate the detector temperature (stability approximately 1mK), the inner sanctum baseplate temperature (stability approx 10mK) and the SIDECAR ASIC temperature (stability approx 10mK). Cooldown time can be as rapid as 4 hrs to 80K, but can be ramped at a slower rate as required by the H2RG SCA using the Lakeshore controller. In order to reduce the radiative thermal load on the inner sanctum, and subsequently on the cryocooler, the IS is surrounded by an actively cooled radiation shield (see Figure **3**). The cooled shield is lightly strapped to the cryocooler head and reaches a temperature of 233K.

Figure 3. Internal view of the SCC-g2 cryostat with radiation shield visible surrounding the inner sanctum. Please see text for component descriptions and dimensions.

The SCC-g2 cryostat also includes a separate high-vacuum valve (NW16) and a micro-pirani vacuum gauge with an operating range from atmospheric pressure down to 10^{-5} Torr. The Stirling cryocooler is attached to the cryostat using a vibration-isolation mounting design that employs a bellows vacuum attachment supported on Sorbathane rings. The GLS-configured Sunpower cryocooler includes two water jackets with one located on the cryocooler head heat-reject ring and one located on the cryocooler body housing the linear motor. An external water chiller is used to remove the approximately 300W of waste heat from the cooler. In Figure **3**, the Stirling cryocooler can been seen mounted on the bottom of the cryostat on its vibration isolation mount. On the front of the cryostat are mounted the vacuum valve and gauge and the cryocooler controller electronics box. The on-cryostat Teledyne interface electronics box is mounted on the backside of the assembly.

4. SELECTION OF A LIGHT SOURCE

4.1 Requirements for NIR LS

As mentioned in the requirements in section 2.1, we sought to cover the NIR (1-5 micron) waveband with a dedicated light source as well as to provide the option to couple an external monochromator in the future. This led to the selection of a dedicated commercial 1-5 micron source to cover the NIR band as well as the provision of an input window for an external source. We also selected an internal cryogenic NIR source based on a nichrome wire concept as an additional option.

4.2 Commercial modular external source

The primary NIR light source for this testbed was selected to be a commercial source which mates to the OTB. In order to adequately cover the 1-5 micron band, we require two separate emitters, namely a ceramic and a tungsten lamp. These are housed in the McPherson dual source reflective condensing module with dual lamp houses, as shown in Figure **4**. The lamp houses use forced air-cooling, safety interlocks, a rear reflector (that improves performance by 40-60%), an iris stop to match the f-number of instrument (f/12) and a common focus mechanism. Both lamps are powered by a common regulated DC power supply which is adjustable with an output ripple of less than 0.05V. It is rated to 300W and can be operated remotely from a 0-8V analog input. The focusing module uses a powered spherical mirror that will flip between each of the two (2) separate sources: a 100W tungsten source for 1 to 2.5 microns and a 20W ceramic emitter for 2.5 to 5 microns. A cylindrical lens on the output removes astigmatism from the off-axis spherical mirror. The McPherson light source will be user selectable to either the shorter (tungsten) or longer (ceramic) part of the NIR

spectrum, as partitioned at 2.5 microns. The following two graphs in Figure 5 show the spectral irradiance (in units of $mW/m^2/nm$ at 0.5 m) of the total area for each of the tungsten and ceramic sources.

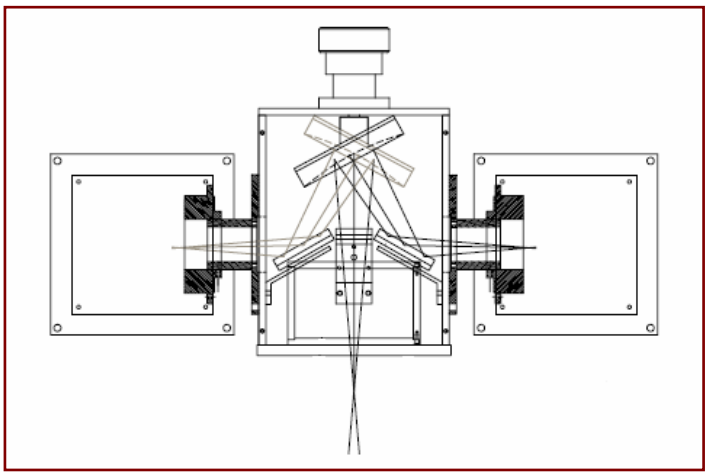

Figure 4. Condensing module with dual lamp houses and Iris Diaphragm (courtesy McPherson, Inc.) showing two separate lamp housing and common flip mirror, iris, and focusing mechanism.

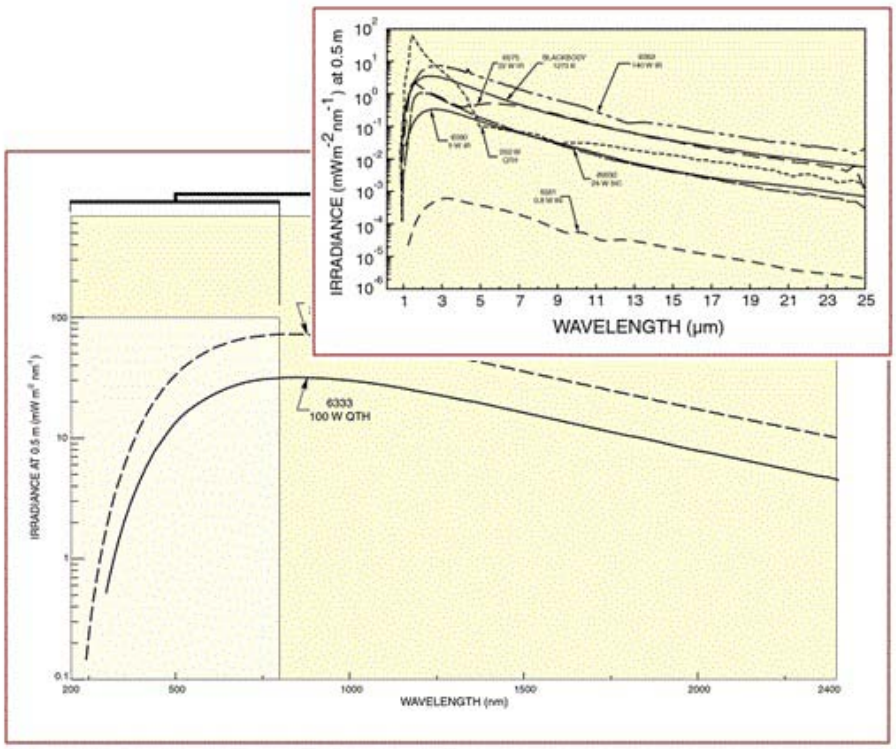

Figure 5. Two graphs showing Tungsten (1-2.5 micron) irradiance (large graph) and ceramic (2.5-5 micron) source irradiance (insert graph) (courtesy Newport Corp.)

It should be noted that spectral irradiance considers each wavelength in the electro-magnetic spectrum separately. The power and source area for each lamp is shown below in Table 1. To roughly calculate whether these sources are suitable, we examine the average irradiance over the spectral band of interest and multiply it by the area of the test sample. We then must multiply the result by the bandpass of the filter. As a limiting case example, the tungsten source will provide 0.2mW/m^2/nm of power at 0.5 meters. Detector literature suggests the NEdT to be less than 18mK, which is equivalent to an NEI of 0.86mW/m^2/nm, giving an order of magnitude of headroom.

Table 1. Summary of Light Source properties

LS Module	Emitter Type	Bandwidth	Power	Source Area
NIR	Tungsten	1-2.5 microns	100W	2.3 x 4.2 mm
NIR	Ceramic	2.5-5 microns	20W	3 x 10 mm

In addition to the McPherson light sources, an optional nichrome wire source can be installed in the OTB cryostat input. The nichrome wire source, shown in Figure 6, will be mounted on a precision cryogenic cross roller slide with rack and pinion gears to drive it. For redundancy, four to six nichrome wires would be installed side-by-side in case one was to burn out. A baffle tube would eliminate stray reflections and a stop would define the f-number to match that of the McPherson sources, nominally f/12. The Aperture wheel would be modified to include a custom tube with a fold mirror and ZnSe re-imaging lens. A similar design is currently under test in the NIC/LMIRcam instrument at the University of Arizona[4].

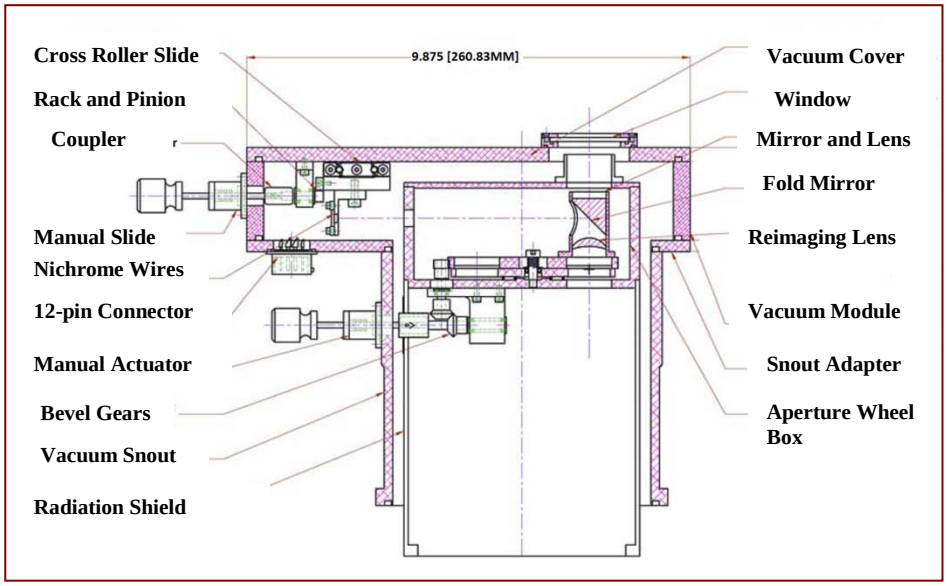

Figure 6. Mechanical drawing of nichrome wire source to be mounted at the OTB front end showing wire selection mechanism, fold mirror and reimaging lens.

5. OPTICAL DESIGN

5.1 Overview of the OTB optical design

As specified in the OTB requirement, section 2.1, the optical design must accommodate transmissive samples in both pupil locations as well as allow for a sample wheel at the intermediate focus. As a consequence, a number of different optical designs were originally explored to satisfy this requirement, including pure refractive, pure reflective, and hybrid designs using spherical and aspherical surfaces. Due to the broad wavelength coverage desired, a reflective design was preferred over a refractive design to eliminate chromatic aberration. In order to control first and third order aberrations

and maintain a reasonable number of elements, aspheric surfaces were necessary. Of the initial optical concepts, two layouts offered clear advantages. These used either off-axis parabolas (OAPs) or biconic aspheric surfaces. In the former case, four OAPs were used to create two pupil planes, an intermediate focal plane, and the final focal plane. In the latter case, two biconics were used. Advantages to each design were evident immediately. While the OAP design created collimated space for each of the pupil planes, the biconic design had the planes in converging beam space. This had the advantage of shrinking the overall size of the optical design, but introduced focal shifts and magnification variations dependent on the thickness of the test samples. Illumination across the pupil planes was apodized as a result.

Other factors considered included cost, manufacturing challenges, lead time, surface figure testing, and alignment complexities. The driving factor was the flexibility to accommodate a range of test sample dimensions. Taking everything into consideration, the OAP design prevailed. Figure 7 shows the final unfolded optical design using four OAP mirrors to create two pupils and an intermediate focal plane. Although many alternative configurations were explored using as many as eight additional fold mirrors to decrease the size of the OTB, a total of four fold mirrors provided the best solution.

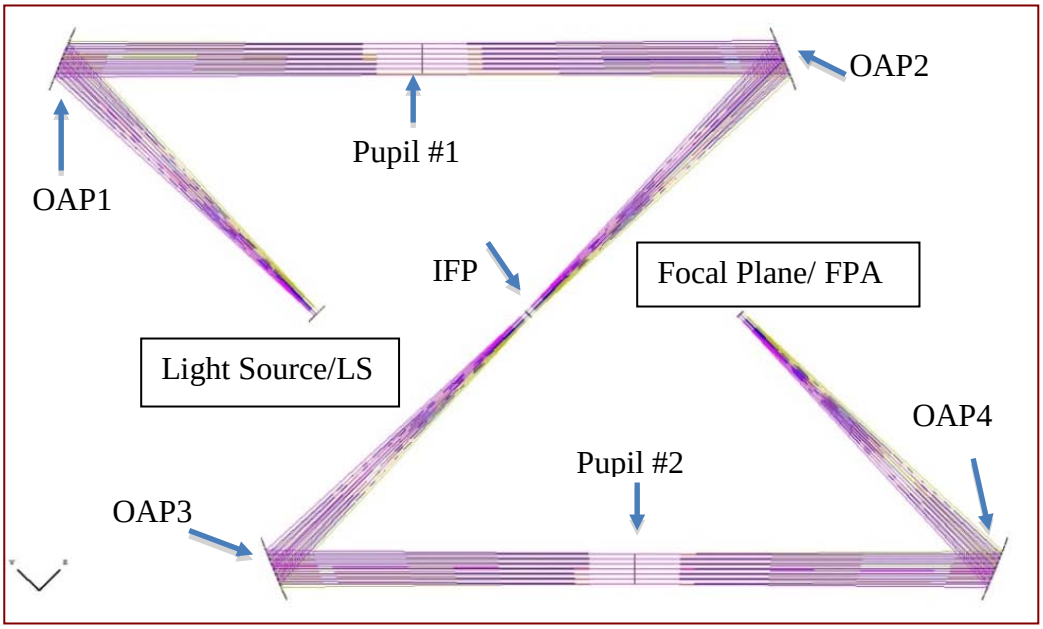

Figure 7. The nominal unfolded OAP optical design showing the four OAPs, the two collimated spaces and the intermediate focal plane. The layout is a 1:1:1 imager and is completely symmetrical. Indicated are light source (LS), intermediate focal plane (IFP), Focal plane, and two pupils in the collimated spaces.

5.2 Optical design performance specifications

The resulting optical design of the OTB is effectively a 1:1:1 relay system. The OAPs have about 1-meter radius of curvatures and create a diffraction limited f/12 system. The geometrical spot diagrams are shown below in Figure 8 for the detector plane. Airy disc radii are shown for the mid-band wavelength of 3 microns.To evaluate performance of the collimated spaces (pupil planes) created by the OAPs, footprint and afocal spot diagrams were used. Unlike the geometrical spot diagrams (measured in telecentric object space with an f/12 input beam) which have units of microns, the afocal spot diagrams (Figure 9) use a collimated input beam and have units of milliradians. Performance is well within the diffraction limit.

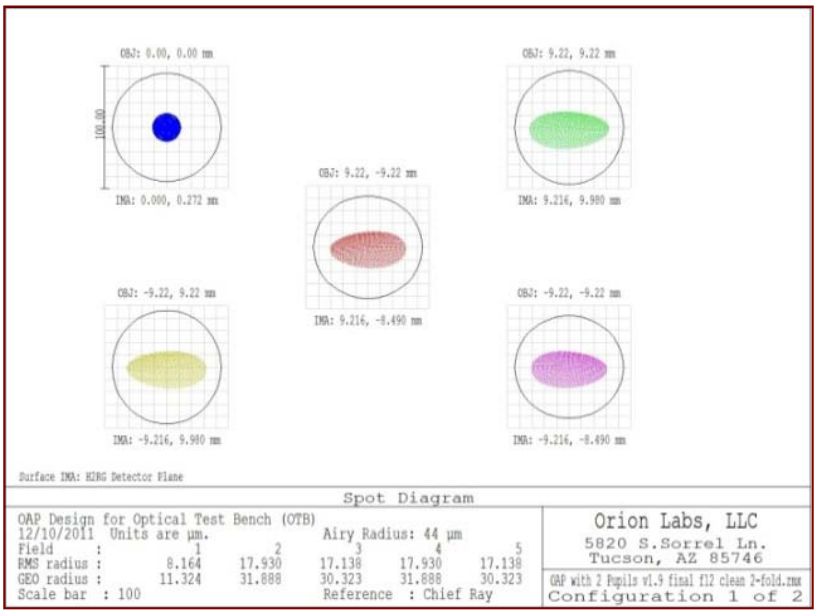

Figure 8. Geometrical spot diagrams of final focal plane indicating diffraction limited performance.

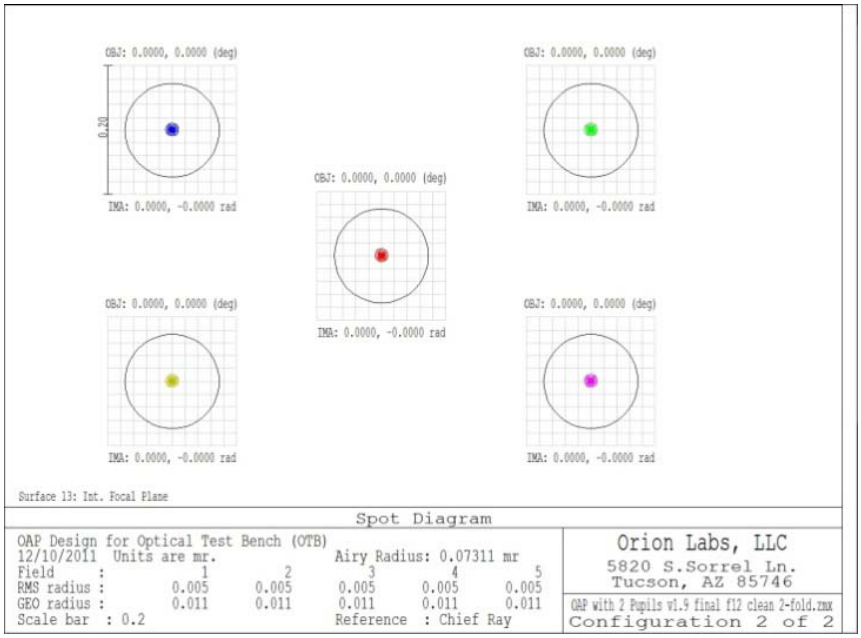

Figure 9. Geometrical spot diagrams of the first pupil plane in afocal mode .

In order to determine the true performance of the optical system, diffraction must be taken into account. A good representation is illustrated in the ensquared energy plot below (Figure 10). The curve shows the fraction of enclosed energy as a function of half-width distance from the centroid, measured in microns and using square rather than circular geometries. For the purposes of the plot, a radial distance of 4 pixels was chosen. As an example, at the 2-pixel (36µm)

distance, the on-axis performance is 98.7 percent of the diffraction limit. In other words, 98.7 percent of the energy from the source is captured within a 2-pixel half-width (4x4 pixels).

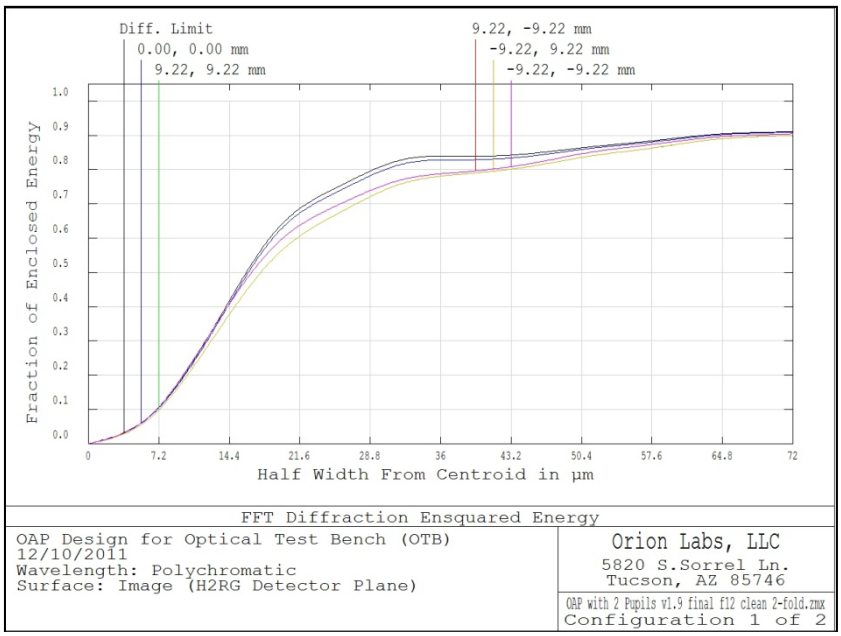

Figure 10. Ensquared energy plot at final focal plane showing on axis performance of 98%.

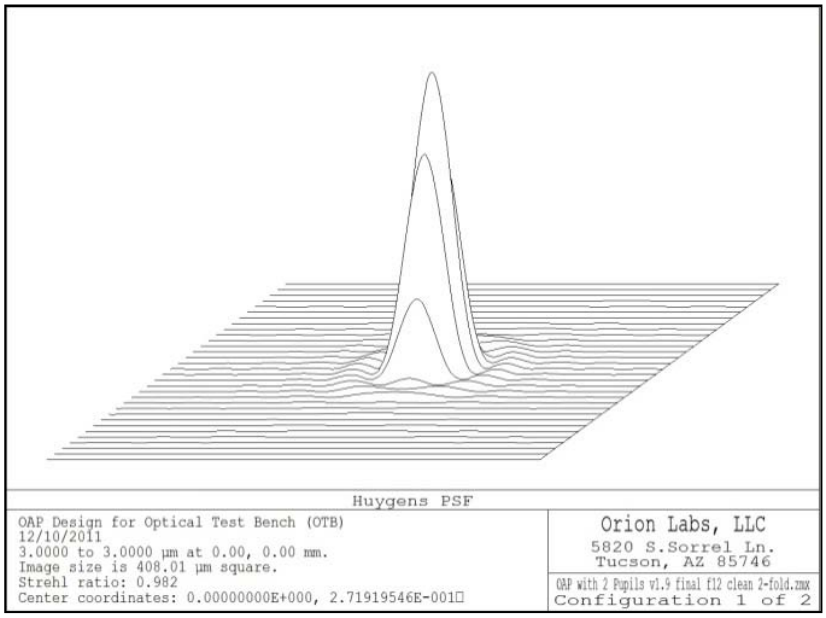

Figure 11. Point spread function at the final focal plane showing an on-axis Strehl of 98%.

Another common measure of optical performance is Strehl ratio. As the plots illustrate the first minimum of the PSF (Airy disc) is well defined at a radial distance of 45 microns. The on-axis Strehl ratio is 98.2 percent as shown in Figure **11**. Off-axis Strehls vary from 90.8 to 91.5 percent for the 18.432mm fields. Performance at the intermediate focal plane improves with near perfect Strehl on-axis. As a result of this optical analysis, we have designed a high precision

optical 1:1:1 relay system as required for this application. With diffraction limited performance across the NIR (1-5 micron) band, we achieve very high on-axis and off-axis Strehls needed to characterize optical components to a high degree of precision.

6. CRYOSTAT DESIGN

The OTB cryostat is a monolithic rectangular case machined from aluminum plate and billet. As seen in Figure 12, this case is mated to a light source input snout on the left. The NIR camera can be seen mounted on the top of the case. The coldhead and vacuum pump-out port are mounted underneath the case as shown in Figure 13. The exit beam can be configured to propagate in the plane of the optical design or bent out-of-plane by adding an additional fold mirror after the last OAP mirror. The latter configuration will be used for initial integration and test at Orion Labs and installation at ETH. The OTB measures approximately 1.6 x 0.8 x 1.5 (L x W x H) meters in the out-of-plane configuration. Due its size and weight, a custom built handling cart will be needed. It will provide mobility with adjustments in height and tilt.

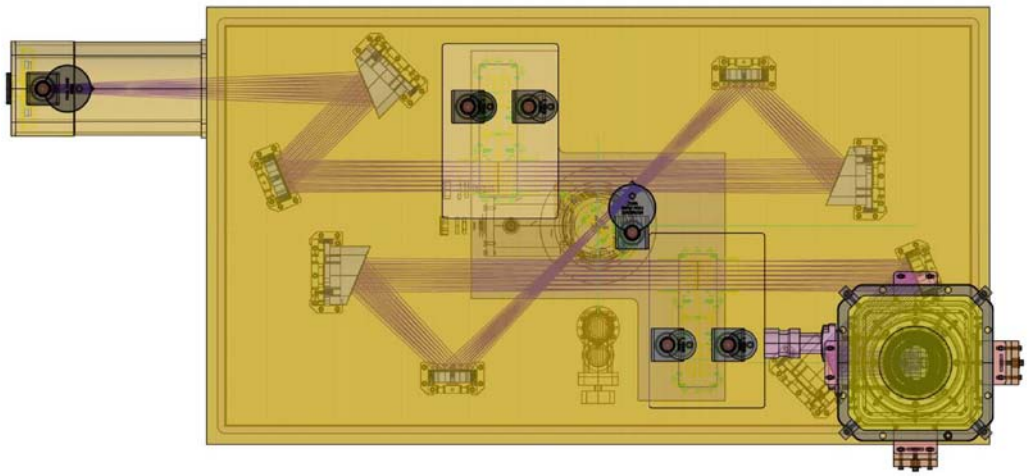

Figure 12. Final packaging of the optical design using four (4) fold mirrors with input snout seen on left. Please see text for description and dimensions.

In principal the OTB and the camera cryostat are two independent systems. They are interfaced to one another through a gate valve that houses a calcium fluoride (CaF_2) vacuum window. The window material was carefully chosen for the NIR operating waveband (1-5 microns). The material is commonly available, inexpensive, not hygroscopic, can be easily anti-reflection coated, and offers adequate mechanical properties for high vacuum use. The interface consists of the gate valve, a vacuum bellows enclosure, flanges, and a separate vacuum pump-out port. The purpose is that if either the OTB or camera cryostats need maintenance, the gate valve can be closed and the interface space purged to atmosphere. One cryostat can be opened while the other remains under vacuum and at cryogenic operating temperature. During sample test mode, the gate valve will be opened to remove the window from the optical beam path, thus eliminating a warm optics from the background and removing any ghosting caused by the plane parallel plate.

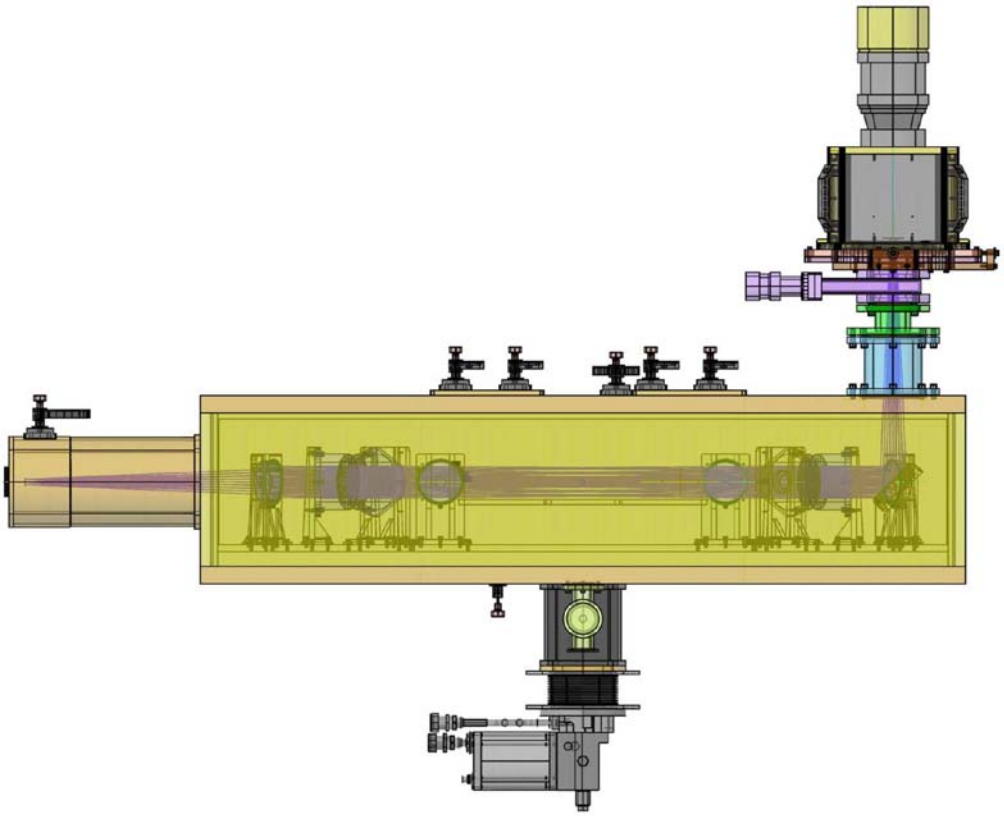

Figure 13. Side view of the OTB with NIR Camera mounted perpendicular to OTB optical axis. The coldhead can be seen mounted on the bottom, and the NIR camera is mounted on top. Optical input snout is left.

6.1 Thermal Design

Given the temperature requirements for the OTB optics, sample wheels, and radiation shield, a thermal heat load analysis was required. The calculations were broken down into several categories including radiative heat path from the case, conductive heat path through mechanism actuators, conductive heat path through wiring harnesses, conductive heat path through the rigid supports, and radiative heat path through the windows. Calculations were based on the mechanical design case and shield dimensions and scaled by twenty percent to size the coldhead and compressor.

In order to simplify some of the calculations, constants for material properties were used instead of recursively calculating them as a function of temperature. The trade-off typically provides a margin of error of ten percent which can be accounted for in the above mentioned scale factor of twenty percent. Experience with previous cryostats provided basic assumptions on total conductive power from wire harnesses and mechanical actuators. A thorough analysis of cross sectional areas, wire material properties, conductivity as a function of temperature, heat capacity as a function of temperature, thermodynamic properties of the various materials used in the conductive path (e.g. aluminum 6061, G-10 fiberglass, OFHC copper, CaF_2, etc) as a function of temperature have been performed for similarly sized instruments and gives confidence that the assumptions for this calculation were reasonable and acceptable.

The most straightforward calculation was the radiative heat path from the case. It contributes the majority of the heat load for the system, particularly on the first stage of the coldhead. First, the surface areas of the inside of the case, coldhead housing, window snout, and radiation shield were computed taking into account all machined holes and detail work. The inside surface area of the OTB was approximately 3.44E+4 cm^2. The radiation shield and coldplate had surface areas of 2.12E+4 and 9.29E+3 cm^2, respectively. To reduce the emissivity of the aluminum surfaces, they will be hand polished and/or super-insulation will be used. The emissivity of all the polished aluminum surfaces is assumed to be 0.03. To calculate the radiative heat transfer from the 300K cryostat case, the following equation was used.

$$BB(T,\varepsilon) = \sigma * \varepsilon * T^4 \quad (1)$$

The blackbody radiation power will have units of $W/cm^2/T^4$. Using σ=5.67E-8 $W/m^2/K^4$ (Stefan-Boltzmann constant), ε=0.03, and T=300K, the total blackbody radiation from the inside of the case is approximately 42.1 Watts. The radiative heat transfer from the 300K case to the 100K radiation shield is given by,

$$P(T1, A1, \varepsilon 1, T2, A2, \varepsilon 2) = \frac{A1 * A2}{A1 + A2} * \left[BB(T1, \varepsilon 1) - BB(T2, \varepsilon 2)\right] \quad (2)$$

So, the total radiative power transferred to the radiation shield is 22.3 W.

Other contributions to the total heat load come from conductive heat paths through the wiring, rigid supports and actuators. Given that the OTB is expected to have a maximum of five (5) actuators (2 on the first stage and 3 on the second), the conductive power is approximately 300 and 900mW, respectively. This is based on a previous calculation from 300 to 77K for one actuator from a similar instrument that used the same actuator design. The temperature differential in our case will be slightly greater, and therefore the power contribution will be greater than 300 mW on the first stage. The actuator itself can be disengaged from the cold mechanism when it is not in use, thereby removing the conductive path completely. Regardless, for the purposes of the analysis, a ten percent increase was added to the 300 mW, bringing the total to 330mW for the first stage. An adjustment factor of twenty percent was used for the second stage, bringing the total conductive power from feedthroughs to 1080mW.

It was estimated that the total number of wires used for the OTB would be between 10 and 28 constantine wires. No heavy coax was needed for the OTB since only temperature sensors, limit and home switches were designed. Their contribution to the conductive heat path was negligible at 12.5 mW. Moreover, in the nominal manual configuration, Home and Limit switches were not used. The only wiring remaining was the housekeeping wiring for the temperature sensors.

Rigid supports underneath the cold plate anchor it to the bottom plate of the case. They provide a direct conductive path to the case and therefore must be fabricated from low thermally conductive materials. G-10 has been used in the past with good success. Its surface area is perforated with large holes to reduce cross sectional area. The number of holes and their size were optimized as much as finite element analysis would allow. The end result was a contribution to the conductive heat transfer for the first stage of approximately 5.4 W for the twelve (12) rigid supports that were expected in the design. Similar supports are used on the top radiation shield to secure it to the upper case. Ten (10) supports are anticipated providing an additional 2.6 W. Each of the filter wheels will be thermally isolated from the 70K cold work surface by a G-10 pad. Nevertheless, total conductive power from the cold work surface to the 30K filter wheel housings is expected to be approximately 0.68W.

6.2 Selection of Cryocooler

The total heat load for the OTB was calculated to be 34.4 Watts. With a 20 percent error margin, the total becomes 41.3 Watts on the first stage of the coldhead. A two-stage coldhead is required to cool the cryostat since the optics, coldplate, and radiation shield will be at one temperature range (70-100K) while the transmissive wheels will be at another (30K). A goal of 70K for the optics and 100K for the radiation shield was assumed. A temperature goal of 30K was assumed for the transmissive wheels. To calculate the thermal load on the second stage of the coldhead, the mass of the mechanisms, differential temperature from surrounding environment, and surface area were needed. The radiative thermal load from the 70K environment to the 30K mechanisms was 0.32 W. These mechanisms will be isolated from the 70K coldplate by G-10 pads. So, the conductive thermal load through the G-10 was 1.72 W. The total heat load for the second stage was expected to be 2.38 W. Adjusted with a twenty percent margin, the total power was 2.86 W.

Direct copper straps from the second stage cold finger to each of the mechanisms will provide effective and controlled cooling.

An appropriately sized coldhead was selected, specifically a CTI model M-1050 dual stage with 9600 compressor. It will provide sufficient cooling at 70K to remove the case dominated heat load. Second stage cooling capacity of 6W (at a first stage temperature of 70K) provides margin to cool the existing mechanisms and any future mechanisms. Further reduction of the operational temperature of the optics may be possible with this coldhead and would further reduce the thermal background signature of the imaging optics.

Five silicon diode temperature sensors will be strategically placed throughout the OTB. Recommended locations include each sample wheel, the first stage cold station, the second stage cold station, and the radiation shield lid. A Lakeshore temperature monitor will record the temperatures while a second controller will be used to control the temperature of the transmissive wheels via heater buttons and a manually operated heat switch. Temperature stability is expected to be +/- 0.2K for each of the sample wheels.

6.3 Mechanisms and internal components

The internal components of the OTB were largely designed in CAD for this custom application. Many of the sub-components designed were modifications from previous cryostats of similar size and complexity. Some of these can be viewed in the 3D cut-away view in Figure 1. The major mechanisms and internal components of the OTB are listed below with notes on their application to give an overview to the number of components in the final assembly.

Cryostat components:

- *Vacuum case* – machined from aluminum plate and billet. The large rectangular box is one piece, no welds. This method costs more but is more reliable and offers the highest degree of precision, design flexibility, and appearance. All exterior surfaces are anodized.
- *Radiation shield* – made from high conductivity. Interior surfaces are blast beaded and black anodized for low background to minimize scatter.
- *Cold work surface* - MIC6 aluminum will be used to guarantee flatness spec. Low background treatment added to work surfaces.
- *Interface flanges* – custom design to interface gate valve to cryostat case. To prevent grounding loops, an electrical isolation barrier is inserted between the two cryostats.
- *Charcoal getter box* – Container is designed to cryo-pump the vacuum inside the cryostat and is designed to cool efficiently and minimize debris.
- *Vacuum valve* – purchase part. It uses stainless steel construction and is very reliable. For high throughput vacuum pump-out, large diameter NW-50 flanges and tubing is used.

Cryocooler interface:

- *Coldhead and compressor* – purchase parts. CTI was chosen mostly due to previous favorable experiences. They provide an excellent selection of high capacity coldheads to match the heat load requirement of the cryostat.
- *Vibration isolation* – the vibrations from the coldhead are isolated via neoprene isolators, a flexible welded bellows assembly, and flexible conductive copper strapping to the cold work surfaces. The bellows assemblies are custom stainless steel units that are obtained from a vendor that specializes in aerospace applications.
- *Copper cooling straps* – made from ultra pure copper foil. The sub-assemblies are customized with a specific number of straps to obtain the optimal cold work surface temperatures. Temperature sensors are placed at suitable locations and can be moved.

Mirror Mounts:

- *Fixed mirror mounts* – for 3-inch diameter flat mirrors, 4 each. Custom machined from 6061 aluminum. Surface treatment is for low background applications, blast beaded and black anodized.

- *Reflective test filter mount (optional)* – 2-position, 2-inch samples. Specifically designed and manufactured by Orion Labs. All parts are CNC machined from 6061 aluminum. Interior surface treatment is for low background applications, blast beaded and black anodized. The mount will be designed to rotate in order to test multiple orders of a grating element.

Mechanisms:

- *Aperture wheel* – 6-position, 2-inch apertures. Specifically designed and manufactured by Orion Labs. All parts are CNC machined from 6061 aluminum. Interior surface treatment is for low background applications, blast beaded and black anodized.
- *Transmissive test filter wheel* – 8-position, 2-inch filters. Specifically designed and manufactured by Orion Labs. All parts are CNC machined from 6061 aluminum. Interior surface treatment is for low background applications, blast beaded and black anodized.
- *Intermediate focal plane wheel* – 6-position, 2-inch apertures. Specifically designed and manufactured by Orion Labs. All parts are CNC machined from 6061 aluminum. Interior surface treatment is for low background applications, blast beaded and black anodized.

All mechanisms were specified to be manually operated for cost considerations, but the design allows for an upgrade path to fully motorized movement. All actuators are custom and will include position indicators. They will have a bayonet style armature that allows for quick engage/disengage motion. This significantly reduces the heat injected directly through conduction from 300K to the 30K cooled mechanism by breaking the path when the mechanism is not in use. In order to change the filters, apertures, or stops in the instrument, the top cover plate of the cryostat must be removed. To facilitate quick and easy access to internal mechanisms, three small hatches will be designed into the larger top plate. Once open, hatches in the top plate of the radiation shield must be removed. Access ports on the sides of all the filter and aperture wheels allow changeability. The mechanism will have to be removed from the cryostat by loosening the screws holding it to the coldplate and disconnecting the Home/Limit switch wiring connector (in the motorized option). The access port is removed by loosening its screws to reveal a clear and open area to clean or change out filters, apertures, or stops. The cryostat design permits upgrade options including the introduction of a turbulence phase plate to simulate atmospheric disturbance, a deformable mirror, and a wavefront sensor.

7. SUMMARY AND OUTLOOK

Our 1-5 micron cryogenic optical test bench is expected to be integrated at ETH Zurich and to see first light in the second half of 2012. We expect that there will be many lessons learned in the final integration and test stages. However, we believe that the selection of high quality components will lead to a reliable system that can be operated by a small staff with great efficiency. It is our hope that this system will be perceived as a valuable asset to the infrared instrumentation community in Europe and around the world. Interested colleagues are welcome to contact us in order to learn more. This laboratory set-up will also be of great value in the education program of ETH students interested in learning about advanced scientific instrumentation. Our ultimate goal is to foster innovation in infrared instrumentation, and to help contribute to the practical realization of novel techniques on ground- and space-based telescopes. We look forward to reporting on future work with this system.

ACKNOWLEDGEMENTS

The authors would like to express their appreciation for helpful discussions with Phil Hinz, Mike Skrutskie and Matt Kenworthy during the development of this concept. We thank Gert Finger at ESO for data on our FPA. We also acknowledge the helpful input of Richard Blank at Teledyne Imaging Sensors, Camarillo, CA and the support of ETH Zurich for this project.

REFERENCES

[1] Kenworthy, M. A., Codona, J. L., Hinz, P. M., Angel, J. R, Heinze, A., Sivanandam, S., "First On-Sky High-Contrast Imaging with an Apodized Phase Plate," ApJ 660, 762-769 (2007).

[2] Mawet, D., et al. "Taking the vector vortex coronograph to the next level for ground- and space-based imaging instruments: review of technology developments in the USA, Japan and Europe," Proceedings of the SPIE, Volume 8151, pp. 815108-815108-14 (2011).

[3] Ives, D. et al. "Performance evaluation of 5 μm cut-off Hawaii-2RG detectors using the fast readout amplifiers," Proceedings of the SPIE, Volume 7742, pp. 77421S-77421S-11 (2010).

[4] Hinz, Phil., "NIC's artificial-source Calibrator (NAC)," Steward Observatory, Internal Report, (2009).

[5] Sidick, E., et al. "Performance of TPF's high-contrast imaging testbed: modeling and simulations," Proceedings of the SPIE, Volume 6265, pp. 62653L (2006).